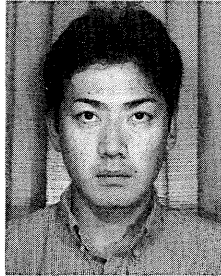


AN INTEGRATED COMPUTATIONAL SYSTEM FOR
MASS/ENERGY GENERATION, TRANSPORT, AND
MECHANICS OF MATERIALS AND STRUCTURES

(Translation from Proceedings of JSCE, No.627/V-44, August 1999)



Tetsuya ISHIDA



Koichi MAEKAWA

The authors present an integrated computational system consisting of a 3D FE structural analysis program and a 3D FE thermo-hygro physical analysis system which can model the development and deterioration of concrete materials performance. The thermo-dynamic process provides solutions for temperature, pore pressure, pore distributions, and other material properties in both 3D space and time. By passing this information to the structural mechanics process, the stress and damage to RC members caused by temperature changes and shrinkage can be obtained. The generation of cracks changes the material properties of mass transport, which are controlled by thermo-physics. This proposed integrated system can be used for the simultaneous evaluation of overall structural and material performances without distinguishing between structure and durability.

Keywords: Durability, structural performance, parallel computation, crack, mass transport

Tetsuya Ishida is an assistant lecturer in the Department of Civil Engineering at University of Tokyo, Japan. He obtained his D.Eng from University of Tokyo in 1999. His research interests cover mass/energy transport phenomena in concrete and the mechanisms of shrinkage and creep of concrete. He is a member of the JSCE and the JCI.

Koichi Maekawa serves as professor in the Department of Civil Engineering at the University of Tokyo, Japan. He obtained his D.Eng. from University of Tokyo in 1985. He specializes in nonlinear mechanics and constitutive laws of reinforced concrete, seismic analysis of structures, and concrete thermodynamics. He is a member of the JSCE and the JCI.

1. INTRODUCTION

At an early age, cementitious materials change in volume as a result of material-related factors such as heat generation, autogenous shrinkage and drying shrinkage. These volume changes cause internal stresses in a restrained RC member and sometimes induce cracking, which accelerates the migration of moisture and ions. This results in accelerated steel corrosion and hence reduced durability performance of RC structures [16][17][18][19]. Consequently, in order to evaluate various measures of structure performance over time, it is necessary to quantify the magnitude of these volume changes, the amount of internal stress and damage that results in RC members, and the characteristics of mass transport in the cracked concrete. It has to be also noted that there is a strong linkage between the mechanical behavior of structural concrete and material quality. The authors understand that a unified approach to the mechanics governing stress and strain fields and the thermo-hygro physics ruling mass and energy transport associated with thermo-dynamic equilibrium would serve as a technique for ensuring overall concrete structure performance as well as concrete performance over the life-span of a concrete structure [1].

In most past design methodologies, structure serviceability and material performance have been treated separately. In this paper, the unification of mechanics and thermo-dynamics of materials and structures is tackled to demonstrate the potential and future direction of research and development.

The volume change of cementitious materials at an early age is dependent on the mix proportion, powder composition, curing, and environmental conditions. In the proposed system, the volume change is modeled from material parameters related to hydration, moisture, and pore structure development using 3D FE code DuCOM [2]. The induced stress and damage to the RC member caused by this volume change is influenced by the shape and the size of the target structure, restraint conditions, material stiffness, and strength. By providing solutions for material properties such as strength, elastic modulus, temperature, water content, and pore structure to the structural analysis program COM3 [3][15] at each step, the stress and the damage can be obtained. The generation of cracks alters the material properties in mass transport characteristics controlled by the thermo-physics system. Though each component in this system is crudely simplified and further progress and development is still needed to accomplish a complete system, the authors aim to show that it is possible to develop a system dynamics for micro-scale pore structure formation and macro-scale defects and structural deformation.

2. OUTLINE OF FE PROGRAMS

2.1 Thermo-hygro physics for concrete performance – the DuCOM sub-system -

In order to trace the early-age development of cementitious materials, it is necessary to consider the inter-relationships among the hydration, moisture transport, and pore-structure development processes. The authors have been developing a 3D FE analysis program code-named DuCOM that simulates these phenomena. This section simply summarizes the overall schemes of this program, since details are presented in a published book [2].

The overall computational scheme is shown in Fig.1. The constituent material models are formulated based on microphysical phenomena, and they take into account the inter-relationships in a natural way. The inputs required in this scheme are mix proportion, powder material characteristics, casting temperature, geometry of the target structure, and the boundary conditions to which the structure will be exposed during its life-cycle. Using the multi-component hydration model, solutions for temperature, degree of hydration, and amount of chemically combined water are obtained [4][5]. By applying the average level of hydration and chemically combined water to a micro pore structure development model, the porosity distribution of hydrated and non-hydrated compounds around reference cement particles is calculated and the surface area of the micro-pores is estimated mathematically [2]. The resulting porosity and pore distributions are used to evaluate moisture conductivity. Using the moisture transport model, which considers both vapor and liquid transports, the pore pressures, relative humidity, and moisture distribution can be obtained [6][7][8]. Here, water consumption due to hydration is considered in solving the mass balance equation, thereby naturally tracing the inter-dependence between moisture transport and

the hydration process.

The chloride distribution in the cementitious materials is calculated using the following formulation [10]. Considering advective transport due to bulk movement of the pore solution phase as well as ionic diffusion due to concentration differences, the flux of chloride ions in the porous medium can be described as,

$$\mathbf{J}_{Cl} = -\frac{\phi S}{\Omega} D_{Cl} \nabla C_{Cl} + \phi S \mathbf{u} C_{Cl} \quad (1)$$

where, $\mathbf{J}_{Cl}^T = [J_x \ J_y \ J_z]$: flux vector of chloride ions [$\text{mol}/\text{m}^2 \cdot \text{s}$]; ϕ : porosity of the porous media; S : degree of saturation of the porous medium; $\Omega = (\pi/2)^2$ accounts for the tortuosity of the 3D pore network, which is uniformly and randomly connected; $\nabla^T = [\partial/\partial x \ \partial/\partial y \ \partial/\partial z]$: the gradient operator; $\mathbf{u}^T = [u_x \ u_y \ u_z]$: advective velocity of ions due to the bulk movement of pore solution phase [m/s]; and C_{Cl} : concentration of ions in the pore solution phase [mol/l]. In the case of chloride ion transport in concrete, S represents the degree of saturation in terms of free water only, as adsorbed and interlayer components of water are also present. Here, it has to be noted that the diffusion coefficient D_{Cl} is a function of ion concentration, since ionic interaction effects will be significant in the fine micro structures at increased concentrations, thereby reducing the apparent diffusive movement driven by the ion concentration gradient [22]. This mechanism, however, is not clearly understood, so we neglect the dependence of ionic concentration on the diffusion process in the model. From several numerical sensitivity analysis, a constant value of $3.0 \times 10^{-11} \text{ [m}^2/\text{s]}$ is adopted for D_{Cl} .

The first term on the right-hand side of Eq. (1) expresses the diffusion of ions, whereas the second term describes advective transport due to the bulk movement of condensed pore water. The advective velocity of chloride ions might also be dependent on the ion concentration, as with the diffusion coefficient. In this paper, however, we assume that the velocity vector of ions is equal to that of liquid pore water, since there is not enough experimental data to establish a model for this aspect.

$$\mathbf{u} = \mathbf{u}_w \quad (2)$$

where, \mathbf{u} : advective velocity of chloride ions; and \mathbf{u}_w : advective velocity of condensed water in pores, which is dependent on relative humidity and moisture content in pore structures.

It is well-known that chlorides in cementitious materials have free and bound components. The bound components exist in the form of chloro aluminates and adsorbed phases on the pore walls, making them unavailable for free transport. It has been reported that the amount of bound chlorides would depend on the binder, the electric potential of the pore wall, and the pH of the pore solution. However, the exact mechanism is still not clear. In this paper, the free and bound components of chlorides under equilibrium conditions are tentatively expressed by the following empirical equations proposed by Maruya, et al. as [11],

$$\alpha_{fixed} = \begin{cases} 1 & C_{tot} \leq 0.1 \\ 1 - 0.35(C_{tot} - 0.1)^{0.25} & 0.1 \leq C_{tot} \leq 3.0 \\ 0.543 & 3.0 \leq C_{tot} \end{cases} \quad (3)$$

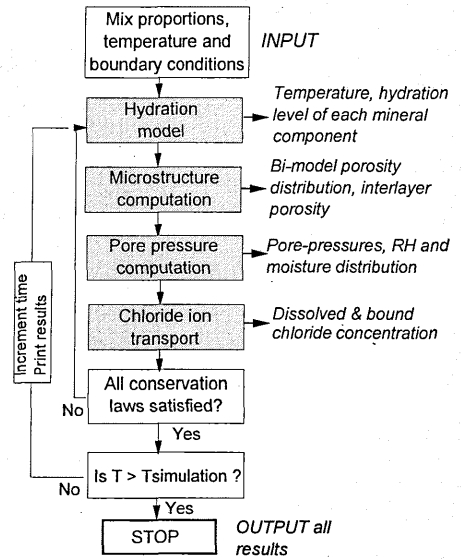


Fig.1 Framework of DuCOM thermo-hygro physics

where, C_{tot} : total chloride content [wt% of cement] ($=C_{free} + C_{bound}$, amount of free chloride and bound chloride, respectively); $\alpha_{fixed} = C_{free} / C_{bound}$: equilibrium ratio of fixed chloride component to total chloride ion component.

By solving the mass balance equation in terms of free chloride ions with the above formulations, the distribution of bound and free chloride ions in cementitious materials can be obtained at any arbitrary stage.

2.2 Continuum mechanics of materials and structures – the COM3 sub system -

On the basis that structures are exposed to low level of stress under normal conditions, we assume that linear creep constitutive equations including temperature/shrinkage strain and creep strain can be written as,

$$\varepsilon_v = \frac{1}{3K} \int (1 + \varphi) d\sigma_v + \varepsilon_T + \varepsilon_{sh} \quad (4)$$

$$e_{ij} = \frac{1}{2G} \int (1 + \varphi) dS_{ij} \quad (5)$$

where, ε_v : average volumetric strain; σ_v : average volumetric stress; S_{ij} : deviatoric stress; e_{ij} : deviatoric strain; K : bulk modulus; G : shear modulus; φ : creep coefficient; ε_T : unrestrained strain due to temperature; ε_{sh} : unrestrained shrinkage strain due to pore pressure.

The unrestrained strain due to temperature and that due to pore pressure at each time and each point are obtained by calculation from material parameters in DuCOM, such as temperature, pore pressure, water content, and pore structure [9]. This calculated strain is passed to COM3. As a result, the thermal stress due to temperature gradient, the shrinkage stress due to self-desiccation/moisture loss, and combinations of these are implicitly considered by this system. The strain tensor can be described as,

$$\begin{Bmatrix} \varepsilon_{xx} \\ \varepsilon_{yy} \\ \varepsilon_{zz} \\ \varepsilon_{xy} \\ \varepsilon_{yz} \\ \varepsilon_{zx} \end{Bmatrix} = [D'] \begin{Bmatrix} \sigma_{xx} \\ \sigma_{yy} \\ \sigma_{zz} \\ \sigma_{xy} \\ \sigma_{yz} \\ \sigma_{zx} \end{Bmatrix} + [D'] \begin{Bmatrix} \int \varphi d\sigma_{xx} \\ \int \varphi d\sigma_{yy} \\ \int \varphi d\sigma_{zz} \\ \int \varphi d\sigma_{xy} \\ \int \varphi d\sigma_{yz} \\ \int \varphi d\sigma_{zx} \end{Bmatrix} + \begin{Bmatrix} \varepsilon_T + \varepsilon_{sh} \\ \varepsilon_T + \varepsilon_{sh} \\ \varepsilon_T + \varepsilon_{sh} \\ 0 \\ 0 \\ 0 \end{Bmatrix} \quad (6)$$

where, $[D'] =$,

$$\begin{bmatrix} \frac{1}{3} \left(\frac{1}{3K} + \frac{1}{G} \right) & 0 & 0 & 0 & 0 & 0 \\ 0 & \frac{1}{3} \left(\frac{1}{3K} - \frac{1}{2G} \right) & 0 & 0 & 0 & 0 \\ 0 & 0 & \frac{1}{3} \left(\frac{1}{3K} - \frac{1}{2G} \right) & 0 & 0 & 0 \\ 0 & 0 & 0 & \frac{1}{3} \left(\frac{1}{3K} + \frac{1}{G} \right) & 0 & 0 \\ 0 & 0 & 0 & 0 & \frac{1}{3} \left(\frac{1}{3K} + \frac{1}{G} \right) & 0 \\ 0 & 0 & 0 & 0 & 0 & \frac{1}{3} \left(\frac{1}{3K} + \frac{1}{G} \right) \end{bmatrix} \quad (7)$$

Symm.

Solving the equation (6) for stress $\{\sigma\}$ gives the basic equation in matrix form as,

$$\{\sigma\} = [D]\{\varepsilon\} - \left\{ \int \varphi d\sigma \right\} - [D]\{\varepsilon_T + \varepsilon_{sh}\} \quad (8)$$

where, $[D]$: stress-strain matrix. Before cracking, the elastic modulus in matrix D is obtained from the calculated hydration level at each gauss point in each element. As for the judgment of cracking in the stress field, if the principal tensile stress at any gauss point exceeds the tensile strength, we assume that a crack would occur at that point. A tensile model of cracked concrete with tension softening as proposed by Okamura [14] is introduced in this study.

$$\sigma_i = \sigma_i(\varepsilon_i; c) = f_i \left(\frac{\varepsilon_{ni}}{\varepsilon_i} \right)^c \quad (9)$$

where, σ_i : mean tensile stress normal to cracks; f_i : tensile strength of concrete; ε_i : tensile strain normal to cracks; ε_{ni} : cracking strain of concrete; c : stiffening factor. The softening behavior of the cracked concrete is modeled by changing the parameter c , which expresses the sharpness of the tension-softening curve. Parameter c can be set at 0.4 for RC concrete with ordinary deformed bars, whereas the value for plain concrete can be obtained from the concrete's fracture energy and the element size [14] (Fig.2).

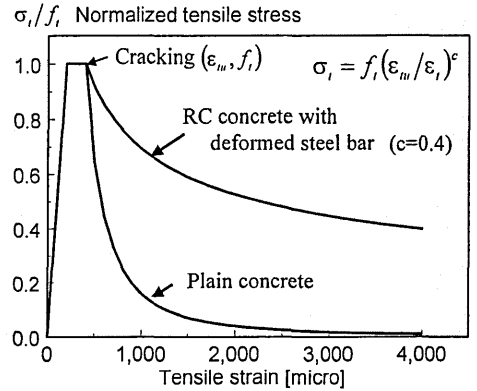


Fig.2 Tension softening model for cracked concrete

Crack propagation due to drying shrinkage involves the generation and growth of smeared micro cracking over the surface, and stress relaxation occurs as a result of micro cracking. It has to also be considered that local cracking between the paste matrix and aggregate will occur [24]. In past research, the generation and propagation of micro cracking was evaluated in terms of local fracture energy [23], but no established theory exists for this behavior. Therefore, in this investigation, we use the above tension-softening model as applied to macroscopic RC members in order to evaluate the stress relaxation after shrinkage cracking [14].

As for the creep coefficient in equations (4) and (5), we adopt the Bazant-Panula formulation [20].

$$\varphi(t, t_0) = \varphi^T \left(t_e^{-m} + \alpha \right) (t - t_0)^{\eta^T} \quad (10)$$

where, t : time [day]; t_0 : loading period [day]; φ^T : coefficient representing the effect of mix proportion and temperature, t_e ; η^T : coefficient representing the effect of temperature history; m : coefficient representing the effect of compressive strength; and α : coefficient representing the effect of water-to-cement ratio.

Strictly speaking, the above model is not well suited to stress analysis under drying conditions, since this creep function represents only basic creep. Still, in this paper, creep function given by eq. (10) is tentatively adopted for the calculations that follow, since we focus mainly on the validity of the proposed method from the viewpoint of numerical analysis.

The authors have been working on another constitutive law that is able to describe time-dependent behavior in terms of deformation and internal stress, as well as the fracture phenomena of restrained structures, for arbitrary thermo-dynamical states. For a detailed discussion of this, see the published paper [21].

3. DUAL PARALLEL PROCESSING OF THERMO-PHYSICS AND STRUCTURAL MECHANICS

For numerical evaluation of overall structural and material performance, we propose parallel processing of two coupled sub-systems as shown in Fig.3. The main feature of this system is that perfect two-way communication is available between the structural mechanics and material characteristics, whereas in conventional thermal stress analysis, material parameters such as temperature rise are passed to the structural analysis in only a one-way transfer.

This system can be embodied in a multitasking operating system such as UNIX or Windows. In this framework, constituent sub-systems with different governing schemes for solving the various governing equations, do not have to be combined into a single process. The operating system manages the tasks of each system, and the two sub-systems are connected by a high-speed signal bus or network so as to share the common data.

First, material properties are calculated by DuCOM. After one step of execution, the calculated results for temperature, water content, pore pressure, pore structure, stiffness, and strength are stored in the common data area. A signal to begin execution is then sent to the sleeping process (COM3). COM3 becomes active and reads the information from the common data area, using it to perform the stress computation. In this analysis, the damage level of the RC member is obtained, and the calculated results are written to the common area after execution. These steps are continued till one of the processes completes its computation. Following this procedure, each FE program can share computational results between the two systems at each gauss point in each finite element.

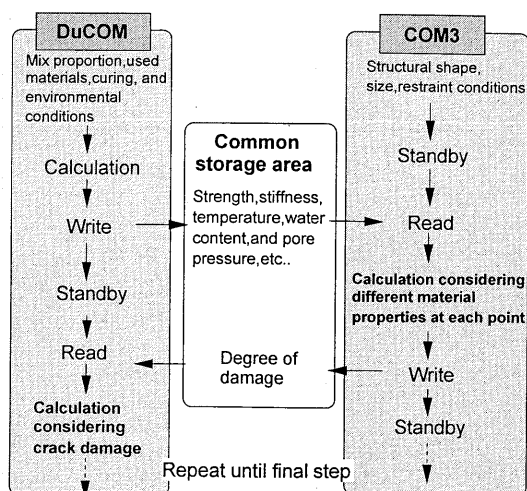


Fig.3 Coupled 3D-FEM scheme of solution for hydration, moisture transport, and structure formation problem in concrete

The chief advantage of unifying the material and structural analysis processes in this manner is the numerical stability of an explicit scheme. Furthermore, this multi-tasking coupled method enables engineers to easily link independently developed computer codes, even if they are in different computer languages and based on different algorithms. As a matter of fact, only slight modification is required for data exchange with the common memory space through high-speed bus, and a short system management program alone is needed.

4. Numerical Simulations

4.1 Moisture distribution in cracked concrete

Using the proposed computational system, numerical simulations of moisture loss in cracked concrete were carried out. It has been reported that there should be a close relationship between moisture conductivity and the damage level of cracked concrete; that is, moisture conductivity should be dependent on the crack width or the continuity of each crack [16][17][18][19]. The proposed system, in which information is shared between the thermo-hygro and structural mechanics processes, is able to describe this behavior quantitatively by considering the inter-relationships between moisture conductivity and cracking properties. However, to check the validity of the proposed system itself, three rough assumptions of moisture conductivity after cracking were made as shown in Fig.5: conductivity after cracking rises by ten times (Case I) and fifty times (Case III) compared with that before cracking, and it increases proportionally to the tensile strain of the cracking elements (Case II). Creep behavior after cracking is not considered, since deformation due to cracking would be large enough to make creep negligible. The analysis can, however, consider the time-dependent behavior of average strain, including the width of cracking as shrinkage increases.

The target structure in this analysis was a concrete slab, which has a 30% water-to-powder ratio using medium heat cement. The volume of aggregate was 70%. After 3 days of sealed curing, the specimen was exposed to 50%RH. Figure 4 shows the mesh layout and the restraint conditions used for this analysis.

Figure 6 shows the cracked elements, the distribution of moisture, and the normalized tensile

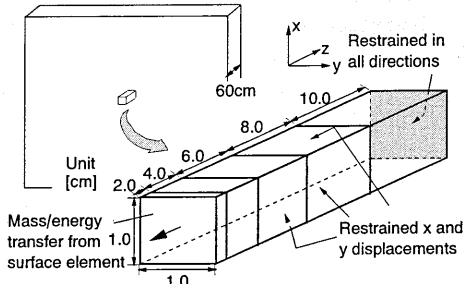


Fig.4 Mesh layout used for FE analysis

Ratio of moisture conductivity after cracking to that before cracking

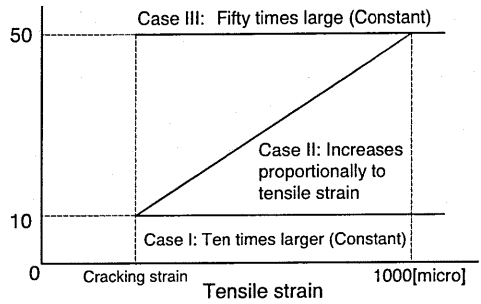


Fig.5 Moisture loss behavior for different drying conditions

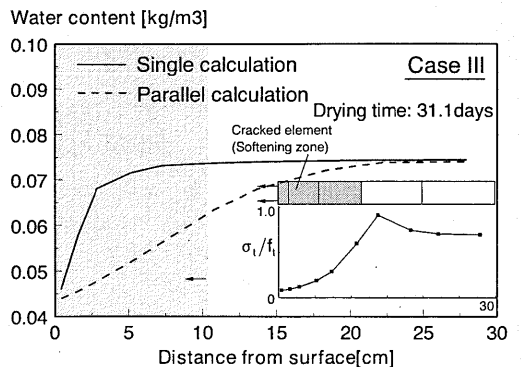
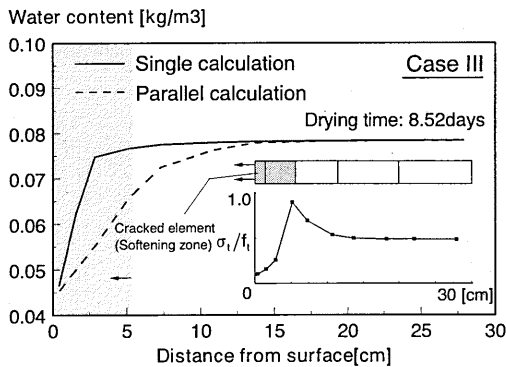
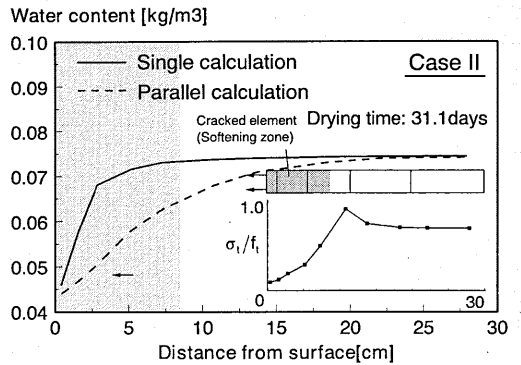
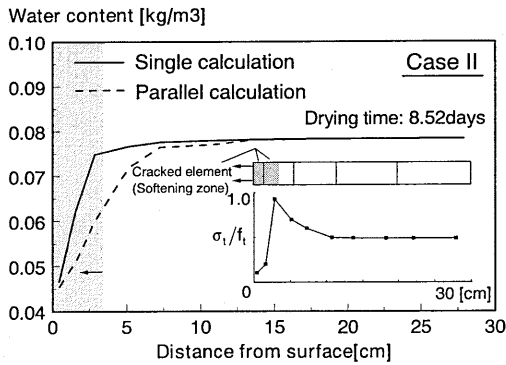
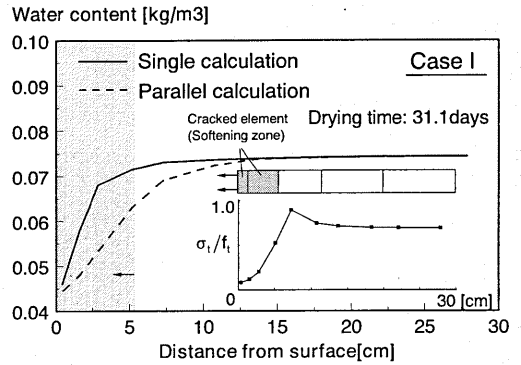
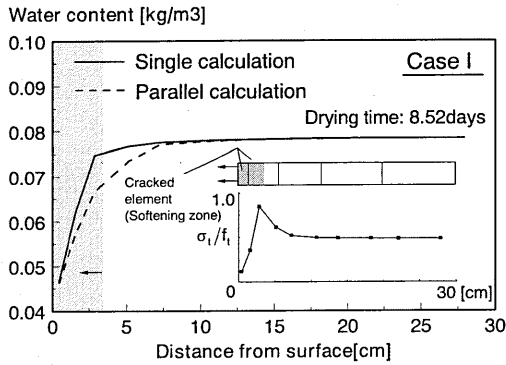


Fig.6 Moisture and internal stress distribution in concrete exposed to drying conditions

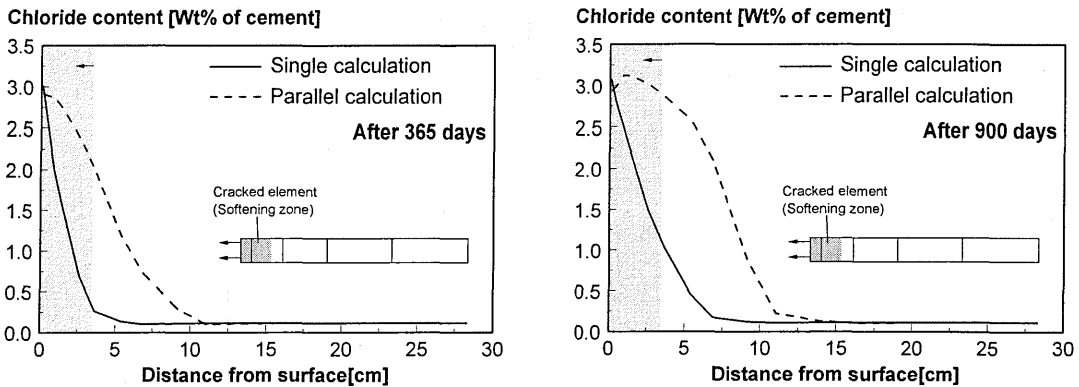


Fig.7 Chloride content in concrete exposed to drying conditions

stress at each point from the boundary surface exposed to drying conditions. The moisture distribution calculated without stress analysis is also shown in Fig.6. As these results show, cracking begins from an element near the surface and the crack progresses internally as drying progresses. It is also clear that the moisture loss rises due to cracking.

4.2 Chloride content in cracked concrete

Next, the migration behavior of chloride ions in cracked concrete was simulated. The size and shape of the target specimen, restraint conditions, and mix proportion are same as in the previous analysis. The specimen was exposed to 0.51 [mol/l] chloride ions under alternating dry (7 days) and wet (7 days) cycles. The distribution of chloride ions inside the concrete after 365 days and 900 days was as shown in Fig.7.

In this analysis, we assume that the liquid conductivity of concrete after cracking is ten times that of non-damaged concrete. When a structure is exposed to wetting conditions, there is a flux of liquid water from outside to inside, and the chloride ions are transported by this flux. The analytical results indicate that chlorides move deep inside the concrete when cracking is considered. It should be noted, however, that the ratio of conductivity after cracking to that before cracking does not have any physical meaning. To check the validity of the proposed system, the simplest assumption was adopted in the analysis.

4.3 Ingress of chloride ions into RC beam damaged by external loading

The final test case was a numerical simulation of the ingress of chloride ions into an RC beam damaged by external loading. Figure 8 shows the size of the beam, the layout of the FE mesh, and the loading conditions used in this analysis. The reinforcement ratio was 0.96%. For the FE analysis of RC structures with a concentrated arrangement of reinforcement, An et al. propose an analytical method to differentiate the RC control volume (RC zone) and the plain concrete volume (PL zone), which have different softening/hardening characteristics. The RC zone is specified for concrete confined by reinforcement, whereas the PL zone is applied to areas far away from the steel bars [14]. In this analysis also, we consider two different zones in RC beams to take into account the difference in concrete mechanics near or far from the reinforcing bars (Fig.8). The tension stiffening model is shown in Fig.2. Stiffening factors c for the RC zone and the PL zone were given as 0.4 and 2.0, respectively [14]. As for the mix proportion adopted in DuCOM, the water-to-cement ratio was 45% and the volume of aggregate was 65%. After 7 days of sealed curing, loading was applied with displacement control until a deflection of 0.42[mm] was reached. Figure 9 shows the relationship between load and deflection at the center section, and the cracked element caused by loading.

After loading, the characteristics of behaviors of chloride transport into the damaged RC beam were simulated. The bottom surface of the beam was exposed to a concentration of chloride ions (0.51 [mol/l]) under alternating dry (7 days) and wet (7 days) cycles. Wetting was simulated by an environmental relative humidity of 99%, whereas drying was given as 50%RH. The characteristics

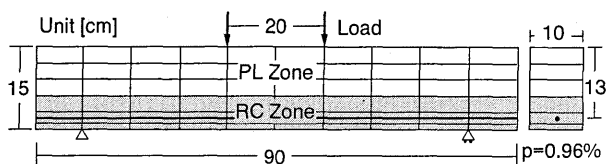


Fig.8 Mesh layout and load conditions used in FE analysis

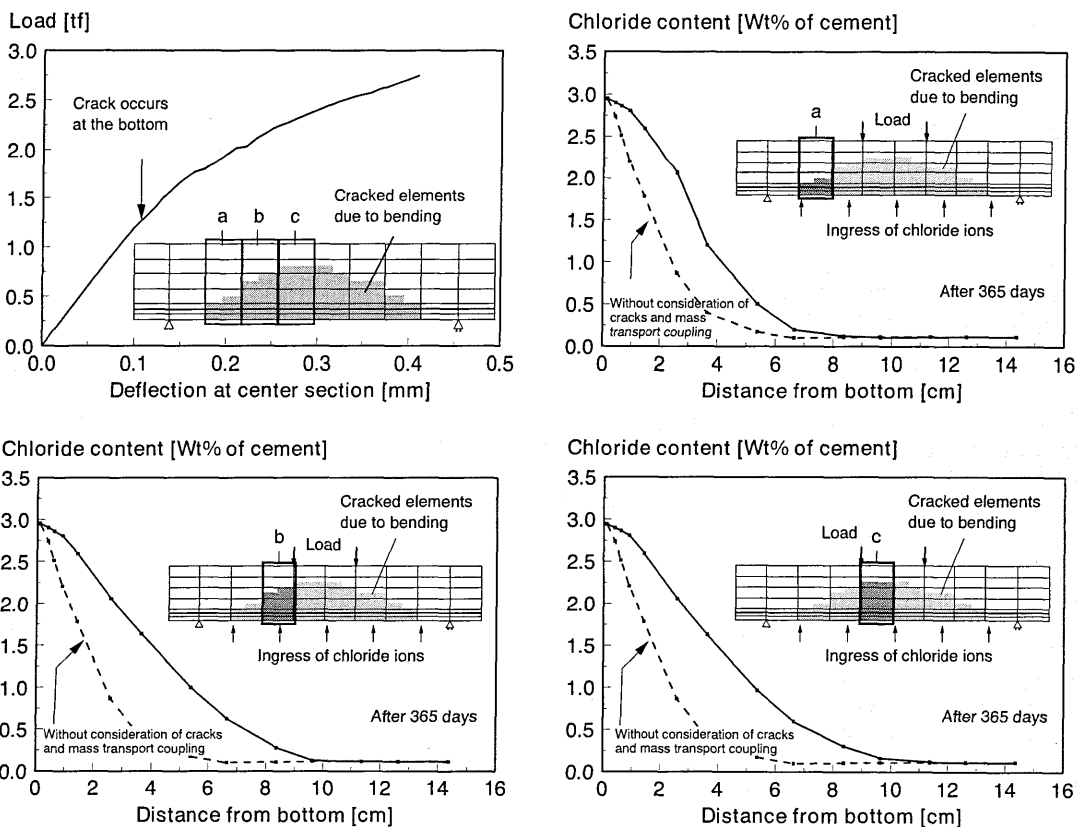


Fig.9 Distribution of chloride ion in damaged RC beam due to external load

of mass transport after cracking can be expected to differ in the RC zone and the PL zone as a result of the different crack density, and we understand that a detailed discussion of this is needed in future. In this analysis, however, the moisture conductivity of the cracked area is roughly assumed to be 10 times that before cracking for the sake of simplicity.

Figure 9 shows the distribution of chloride ions at points a, b, and c. The parallel simulations clearly show deeper ingress of chloride ions up to 100 days as compared to the results when cracking and mass transport coupling are not considered. It can also be seen that the ingress of chloride ions increases near the center section, since in a cracked element the bulk movement of chloride ions in pore water can easily take place.

5. CONCLUSIONS

An integrated computational system for thermo-physics and structural mechanics is proposed. Based on coupling under a multi-tasking operating system, it enables engineers to easily link independently developed computer codes even if different languages and algorithms are used, since each system is managed by the operating system and the calculated results are shared

through a common data area. Though each component in this system is crudely simplified and further development is required to achieve a finished system, the dynamics of micro-scale pore structure formation and macro-scale structural defects and deformations as calculated by this system indicate its potential.

Appendix

The governing equations solved by the proposed system are shown in Figs. a, b, and c. Figure a shows the mass and energy conservation laws which govern the thermo-physics of materials, as well as the balance equations which govern the mechanics of structures. These conservation laws must be satisfied in all material systems and so they apply to the field of concrete materials. Figure a also shows the mass, energy, and momentum transport terms, and sink term, for the above equations. These governing equations are derived from the specific characteristics of concrete materials. In this system, we neglect momentum transport with mass transport and momentum generation by product and/or loss of mass and energy, since their magnitude would be quite small. Figures b and c show the state, compatibility, and constitutive laws of mass, energy, and solid concrete. These equations are also modeled by considering the specific characteristics of concrete.

Table I shows input values needed for the calculation. In addition to the list in Table I, the x, y, and z-coordinates of each node and the element type/shape of the analytical target are required for the analysis. These input values determine the initial value at time=0, and also determine some of the material constants shown in Table II. Other material constants are taken from experimental results. By solving the above governing equations under given material constants and initial conditions, the variables shown in Table III are obtained in 3D space and the time domain.

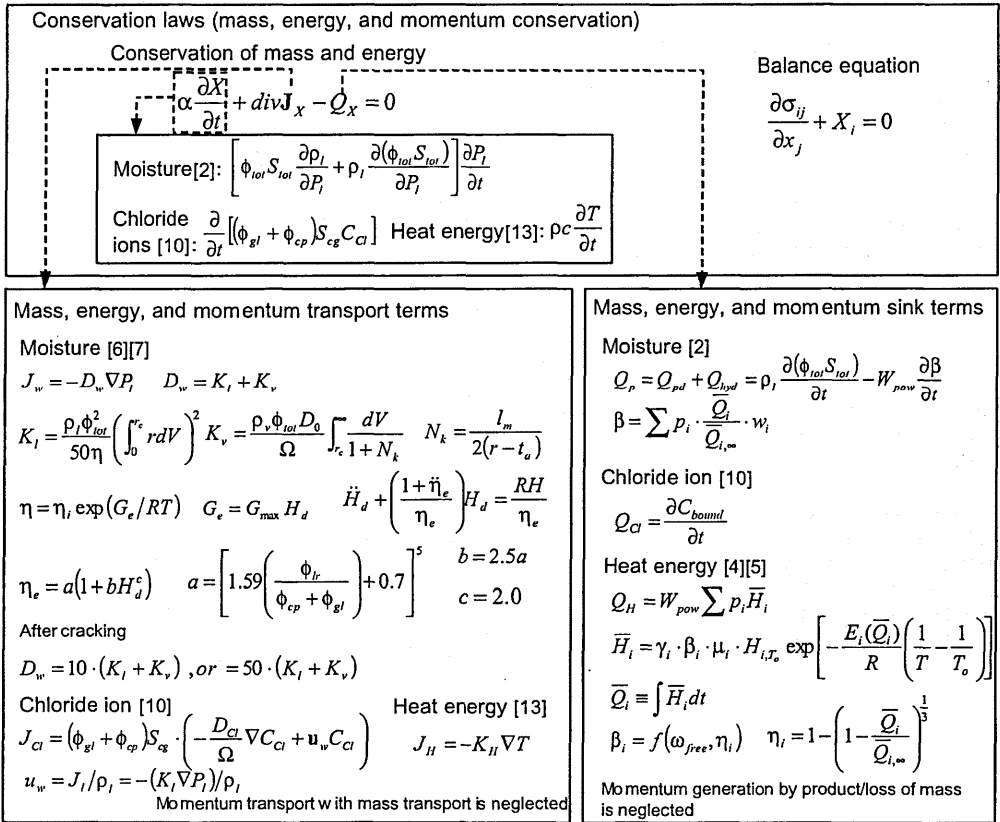


Fig.a Conservation laws, mass/energy transport, and sink term

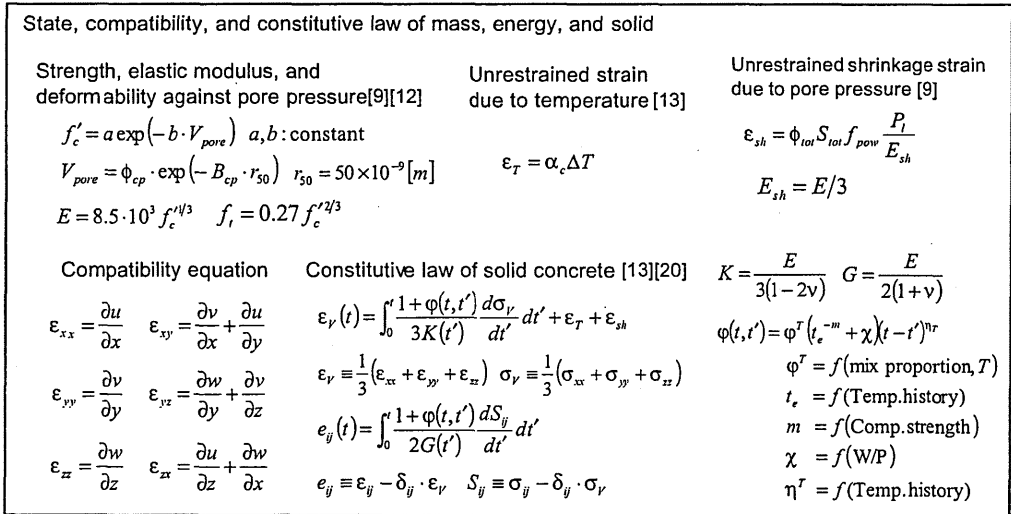


Fig.b State and compatibility law of mass, energy, and solid (No.1)

State, compatibility, and constitutive law of mass, energy, and solid

<p>Pore structure formation [2]</p> $V_s = \frac{\alpha W_{pov}}{1 - \phi_{ch}} \left(\frac{1}{\rho_p} + \frac{1}{\rho_w} \cdot \frac{\beta}{W_{pov}} \right) \quad \phi_{lr} = (t_w s_l \rho_g) / 2$ $\alpha = \sum P_i \cdot (\bar{Q}_i / \bar{Q}_{i,\infty}) \quad \phi_{gl} = V_s \phi_{ch} - \phi_{lr}$ $\phi_{cp} = 1 - V_s - (1 - \alpha) \frac{W_{pov}}{\rho_p} \quad \phi_{tot} = \phi_{lr} + \phi_{gl} + \phi_{cp}$ $\rho_g = \rho_p \rho_w (1 + \beta / W_{pov}) (1 - \phi_{ch}) / (\rho_w + \beta \rho_p)$ $A \delta_m^2 + B \delta_m + C \bar{D}_m + D = 0$ $A = \{n(1 - \phi_{in}) + 3(1 - \phi_{ou})\} / \{3(n + 3)\}$ $B = \{n(1 - \phi_{in}) + 2(1 - \phi_{ou})\} r_0 / (n + 2)$ $C = \{n(1 - \phi_{in}) + (1 - \phi_{ou})\} r_0^2 / (n + 1)^2$ $D = -(\alpha r_0^3 / 3) [\phi_{in} + \beta \rho_p / \rho_w]$	<p>Before contact $\phi_{ou} = 1.0$</p> <p>After contact $\phi_{ou} = 1 - (X + Y) / Z \quad \delta_{max} = k r_0$</p> $X = -n(1 - \phi_{in}) \left[\frac{k^3}{3(n + 3)} + \frac{k^2}{n + 2} + \frac{k}{n + 1} \right]$ $Y = \frac{\alpha}{3} \left[\phi_{in} + \beta \frac{\rho_p}{\rho_w} \right] \quad Z = \frac{k^3}{n + 3} + \frac{2k^2}{n + 2} + \frac{k}{n + 1}$ $s_l = 510 f_{pc} + 1500 f_{sg} + 3100 f_{fa}$ $\zeta = 19.0 f_{pc} + 1.5 f_{sg} + 1.0 f_{fa}$ $SA_c = \frac{3 \bar{D}_m}{\zeta r_0^3 (1 - \phi_{in})} (A \delta_m^2 + B \delta_m + C)$ $SA_l = 2 \phi_{lr} \int_{r_{in}}^{r_{ou}} B_l \exp(-B_l r) d \ln r \quad SA_g = W_s \cdot sa_g$ $\phi(r) = \phi_{lr} + \phi_{gl} \cdot V_{gl} + \phi_{cp} \cdot V_{cp} \quad V_l = 1 - \exp(-B_l r)$
---	--

Thermodynamic equilibrium of mass

<p>Moisture[6][7][8]</p> $P_l = \frac{\rho_l RT}{M_l} \ln RH = -\frac{2\gamma}{r_c}$ $t_n = \frac{0.525 \times 10^{-8} \cdot RH}{(1 - RH / RH_m)(1 - RH / RH_m + 15RH)}$ $RH_m = \exp \left[\frac{-\gamma M_l}{\rho_l RT (r - t_a)} \right]$ $S_{ads} = \int_c^{\infty} \left[1 - \left(\frac{r - t_a}{r} \right)^2 \right] dV$ $S_{cnd} = \int_0^c dV = 1 - \exp(-Br_c) = S_c$ $S_{lr} = RH$ <p>(Wetting stage)</p>	$S_{cnd} = S_c + \int_c^{\infty} \left(\frac{S_c}{V} \right) dV = S_c [1 - \ln S_c]$ $S_{lr} = RH^{0.05}$ <p>(Drying stage)</p> $S_{cnd} = S_c + \int_c^{\infty} \left(\frac{S_{r_{min}}}{V} \right) dV = S_c - S_{r_{min}} \ln S_c$ $S_{lr} = S_{max} RH^{0.05}$ <p>(Drying to wetting stage)</p> $S_{cnd} = S_c + \int_c^{max} \frac{S_c}{V} dV = S_c [1 + \ln S_{r_{max}} - \ln S_c]$ $S_{lr} = 1 + (RH - 1) \left(\frac{S_{min} - 1}{RH_{min} - 1} \right)$ <p>(Wetting to drying stage)</p>	$S_{cg} = S_{ads} + S_{cnd}$ $S_{tot} = \frac{\phi_{lr} S_{lr} + (\phi_{gl} + \phi_{cp}) S_{cg}}{\phi_{tot}}$ $\omega_{free} = \frac{\phi_{cp} S_{cp} (1 - V_g)}{W_{pov}}$
---	---	--

<p>Chloride ion [11]</p> $\alpha_{fixed} = 1 - 0.5(C_{tot} - 0.5)^{0.39}$ 0.141	$C_{tot} \leq 0.5$ $0.5 \leq C_{tot} \leq 4.5$ $4.5 \leq C_{tot}$	$C_{tot} = C_{Cl} + C_{bound}$ $\alpha_{fixed} = C_{bound} / C_{tot}$
---	---	---

Fig.c State and compatibility law of mass, energy, and solid (No.2)

Appendix Table. I List of input values

P_i	Initial pore pressure [Pa]	W_{pow}	Powder weight per unit volume [kg/m ³]
C_{cl}	Initial concentration of Cl ions[mol/l]	V_g	Aggregate volume per unit volume [kg/m ³]
T	Initial temperature [K]	f_{pc}	Weight fraction of Portland cement
p_i	Mass ratio of chemical component of cement (C ₂ S, C ₃ S, C ₄ AF, C ₃ A, gypsum)	f_{sg}	Weight fraction of blast furnace slag
ρ_p	Density of powder materials [kg/m ³]	f_{fa}	Weight fraction of fly ash
W/P	Water-to-powder ratio	p_{sp}	Amount of organic admixture

Table. II List of material constant

ρ_l	Density of liquid [kg/m ³]	ϕ_{ch}	Specific porosity of gel products (=0.28)
ρ_v	Density of saturated vapor [kg/m ³]	ϕ_{in}	Specific porosity of inner products (=0.28)
ρ_c	Heat capacity [kcal/K.m ³]	t_w	Thickness of interlayer porosity (=2.8×10 ⁻¹⁰ [m])
D_0	Vapor diffusivity in free atmosphere [m ² /s]	s_l	Specific surface area of interlayer porosity [m ² /kg]
D_{cl}	Chloride ion diffusivity in pore solution phase [m ² /s]	n	Parameter representing a generic pattern of deposition of products around particle
Ω	Parameter representing tortuosity of pore (= ($\pi/2$) ²)	r_0	Radius of powder particle [m]
η_i	Viscosity under ideal conditions [Pa.s]	ζ	Ratio of volume to the external surface area of a typical hydrate products[nm]
l_m	Mean free path of a water molecule [m]	f_{pc}	Weight fraction of portland cement
G_{max}	Maximum additional Gibbs energy for the activation of flow(=3500kcal/mol)	f_{sg}	Weight fraction of blast furnace slag
K_H	Heat conductivity [kcal/K.m.sec]	f_{fa}	Weight fraction of fly ash
p_i	Mass ratio of chemical component i of cement	r_{eq}	Equivalent spherical cell radius [m]
w_i	Amount of water consumed by chemical component i due to hydration [mol/mol]	sa_g	Specific surface area of hydrates [m ² /kg]
$\bar{Q}_{i,\infty}$	Maximum theoretical specific heat of component i [kcal]	r_m	Minimum radius of pores [m]
W_{po}	Powder weight per unit volume [kg/m ³]	M_l	Molecular mass of liquid [kg/mol]
w	Reduction factor representing the retardation effect on hydration of fly ash and organic admixture	γ	Surface tension of liquid [N/m]
μ_i	Coefficient representing the effect of mineral composition (C ₃ S, C ₂ S) on hydration rate	V_g	Volume of aggregate per unit volume [m ³ /m ³]
T_0	Reference temperature (=293 K)	α_c	Coefficient of linear expansion of concrete [1/K]
R	Gas constant [J/mol.K]	f_{pow}	Fractional volume of powder materials
ρ_p	Density of powder materials [kg/m ³]	δ_{ij}	Kronecker delta
ρ_w	Density of chemically hydrated products [kg/m ³]	ν	Poisson's ratio

Table. III List of variables

t	Time [s]	η_i	Non-dimensional thickness of cluster
-----	----------	----------	--------------------------------------

P_l	Pore pressure [Pa]	V_s	Volume of hydrated products [m^3/m^3]
C_{cl}	Concentration of chloride ions [mol/l]	W_s	Weight of hydrated products [kg/m^3]
T	Temperature [K]	α	Average degree of hydration
J_w	Flux of moisture [$kg/m^2.s$]	ρ_g	Dry density of gel products [kg/m^3]
J_{cl}	Flux of chloride ions [$mol/m^2.s$]	ϕ_{cp}	Capillary porosity
J_H	Flux of heat [$kcal/m^2.s$]	ϕ_{gl}	Gel porosity
D_w	Moisture conductivity [$kg/Pa.m.s$]	ϕ_{lr}	Interlayer porosity
K_l	Liquid conductivity [$kg/Pa.m.s$]	ϕ_{tot}	Total porosity
K_v	Vapor conductivity [$kg/Pa.m.s$]	ϕ_{ou}	Porosity at outermost boundary of the expanding cluster
η	Viscosity of fluid under non-ideal conditions [$N.s/m^2$]	δ_m	Cluster thickness
η_e	Effective non-ideal viscosity of the pore fluid [$N.s/m^2$]	SA_c	Specific surface area of capillary porosity [m^2/m^3]
G_e	Additional energy for activation of flow	SA_g	Specific surface area of gel porosity [m^2/m^3]
H_d	Fictitious humidity parameter	B_i	Porosity distribution parameter
r	Pore radius [m]	RH	Relative humidity
r_c	Pore radius in which the equilibrated interface of liquid and vapor is created [m]	t_a	Thickness of adsorbed layer [m]
V	Normalized pore volume [m^3/m^3]	RH_m	Humidity required to fully saturate a pore
N_k	Knudsen number	S_{ads}	Degree of saturation due to adsorbed water
u_w	Velocity vector of pore solution phase	S_{cnd}	Degree of saturation due to condensed water
J_l	Flux of liquid [$kg/m^2.s$]	S_c	Degree of saturation due to condensed water in virgin wetting path
Q_p	Sink term for moisture balance	r_{max}	Pore radius of the largest pores that experienced a complete saturation in the wetting history [m]
Q_{pd}	Term representing bulk porosity change effects	S_{rmax}	Highest saturation experienced by the porous media in its wetting history
Q_{hyd}	Term representing water consumption due to hydration	r_{min}	Pore radius of the smallest pores that experience emptying out in the drying history [m]
β	Amount of chemical combined water per unit weight of hydrated powder materials [kg/kg]	S_{rmin}	Lowest saturation of porous media in its wet-dry history
\bar{Q}_i	Accumulated heat generation of chemical component i [kcal]	S_{max}	Highest saturation experienced by interlayer porosity in its wetting history
Q_{cl}	Term representing the reduction of free chlorides	S_{min}	Lowest saturation experienced by interlayer porosity in its drying history
C_{bound}	Amount of bound chlorides [mol/l]	RH_{min}	Minimum RH experienced in its drying history
Q_H	Heat generation term	S_{cg}	Degree of saturation of gel and capillary pores
\bar{H}_i	Heat generation rate of clinker component i [$kcal/kg.s$]	S_{lr}	Degree of saturation of interlayer porosity
H_{i,T_0}	Reference heat rate of i -th component at temperature T_0 [$kcal/kg.s$]	S_{tot}	Degree of saturation of total pores
$E_i(\bar{Q}_i)$	Activation energy of component i [$kcal.K/kg.s$]	α_{fixed}	Equilibrium ratio of fixed chloride component to total ion component
β_i	Reduction of probability of contact	C_{tot}	Total amount of chloride ions [mol/l]

	between unhydrated compounds and free pore water		
ω_{free}	Amount of free water	ε_T	Unrestrained strain due to temperature
ε_{sh}	Unrestrained shrinkage strain due to pore pressure	ε_V	Average volumetric stress
E_{sh}	Deformability against capillary stress [Pa]	σ_V	Average volumetric strain
f_c'	Compressive strength [Pa]	e_{ij}	Deviatoric stress
V_{pore}	Volume of capillary pores above 50nm	S_{ij}	Deviatoric strain
E	Elastic module [Pa]	K	Bulk modulus
f_t	Tensile strength [Pa]	G	Shear modulus
X_i	External force in i -direction	ϕ	Creep coefficient
u	Displacement in x-direction	ϕ^T	Coefficient representing effect of mix proportion and temperature
v	Displacement in y-direction	t_e	Coefficient representing effect of temperature history
w	Displacement in z-direction	M	Coefficient representing effect of compressive strength
t'	Loading period [s]	χ	Coefficient representing effect of W/C
ε_{ij}	Strain tensor	η^T	Coefficient representing effect of temperature history
σ_{ij}	Stress tensor		

References

- [1] K. Sakai (Editor): Integrated design and environmental issues in concrete technology, *Proceedings of international workshop in Hakodate*, E&FN SPON, 1995.
- [2] Maekawa, K., Kishi, T., and Chaube, R. P.: *Modelling of Concrete Performance*, E&FN SPON, 1999.
- [3] Okamura, H. and Maekawa, K.: *Nonlinear Analysis and Constitutive Models of Reinforced Concrete*, Gihodo, Tokyo, 1991.
- [4] Kishi, T. and Maekawa, K.: Multi-component model for hydration heating of Portland cement, *Concrete Library of JSCE*, No.28, pp. 97-115, 1996.
- [5] Kishi, T. and Maekawa, K.: Multi-component model for hydration heating of blended cement with blast furnace slag and fly ash, *Concrete Library of JSCE*, No.30, pp. 125-139, 1997.
- [6] Chaube, R.P. and Maekawa, K.: A study of the moisture transport process in concrete as a composite material, *Proceedings of the JCI*, Vol. 16, No.1, pp.895-900, 1994.
- [7] Chaube, R.P. and Maekawa, K.: A permeability model of concrete considering its microstructural characteristics, *Proceedings of the JCI*, Vol. 18, No.1, pp. 927-932, 1996.
- [8] Ishida, T., Chaube, R.P., Kishi, T., and Maekawa, K.: Modeling of pore water content in concrete under generic drying wetting conditions, *Concrete Library of JSCE*, No.31, pp. 275-287, 1998.
- [9] Ishida, T., Chaube, R.P., Kishi, T., and Maekawa, K.: Micro-physical approach to coupled autogenous and drying shrinkage of concrete, *Concrete Library of JSCE*, No.33, pp. 71-81, 1999.
- [10] Maekawa, K. and Ishida, T.: Service-life evaluation of reinforced concrete under coupled forces and environmental actions, *Proceedings of International Conference on Ion and Mass Transport in Cement-based Materials*, 1999 (To be published).
- [11] Maruya, T., Matsuoka, Y., and Msirikul, S.: Simulation of chloride movement in hardened concrete, *Concrete Library of JSCE*, No.20, pp. 57-70, 1992.
- [12] Okamura, H. and Maeda, S: *Reinforced Concrete Engineering*, Ichigaya Syuppan, Tokyo, 1987 (in Japanese).
- [13] Okamura, H., Maekawa, K., and Ozawa, K.: *High Performance Concrete*, Gihodo, Tokyo, 1993 (In Japanese).
- [14] An, X., Maekawa, K. and Okamura, H.: Numerical simulation of size effect in shear strength of RC beams, *Proceedings of JSCE*, No.564, V-35, pp.297-316, 1997.
- [15] Maekawa, K., Irawan, P., and Okamura, H.: Path-dependent three-dimensional constitutive

- laws of reinforced concrete - formation and experimental verifications, *Structural Engineering and Mechanics*, Vol.5, No.6, pp.743-754, 1997.
- [16] T. Shimomura, Modelling of Initial Defect of Concrete due to Drying Shrinkage, *Concrete Under Severe Conditions 2*, CONSEC 98, Vol.3, pp.2074-2083, 1998.
- [17] T. Nishi, T. Shimomura and H. Sato, Modeling of Diffusion of Vapor Within Cracked Concrete, *Proceedings of the JCI*, Vol. 21, No. 2, pp.859-864, 1999 (in Japanese).
- [18] Bazant, Z. P., Sener, S., and Kim, J.: Effect of cracking on drying permeability and diffusivity of concrete, *ACI materials journal*, No.84-M35, pp.351-357, 1987.
- [19] Oshita, H. and Tanabe, T.: Mathematical modeling for permeability behavior of non-homogeneous material and its applicability, *Concrete Library of JSCE*, No.29, pp. 69-92, 1997.
- [20] Bazant, Z. P. and Panula, L.: A note on amelioration of the creep function for "Improved dischinger method", *Cement and Concrete Research*, Vol.8, pp.381-386, 1978.
- [21] Mabrouk, R., Ishida, T., and Maekawa, K.: Solidification model of hardening concrete composite for predicting autogenous and drying shrinkage, *Autogenous shrinkage of concrete edited by Ei-ichi Tazawa*, pp.309-318, E&FN SPON, 1998.
- [22] Gjorv, O.E. and Sakai, K.: Testing of chloride diffusivity for concrete, *Proceedings of the international conference on concrete under severe conditions*, CONSEC 95, pp.645-654, 1995.
- [23] Alvaredo, A.M. and Wittmann, F.H.: Shrinkage as influenced by strain softening and crack formation, creep and shrinkage of concrete, *Proceedings of the fifth international RILEM symposium*, pp.103-113, E&FN SPON, 1993.
- [24] Mier, J.G.M.van.: Fracture processes of concrete, CRC press, 1997.